ASTFE
American Society
of Thermal and Fluids Engineers

7th Thermal and Fluids Engineering Conference (TFEC)
April–May, 2022
Partially Online Virtual and in Las Vegas Conference

TFEC-2022-40927

MATHEMATICAL MODELING OF A THERMOELECTRIC GENERATOR UNICOUPLE

Sarah E. Wielgosz,[1] Shane P. Riley,[1] Kevin Yu,[2] Michael J. Durka,[2] Bill J. Nesmith,[2] Fivos Drymiotis,[2] Jean-Pierre Fleurial,[2] Matthew M. Barry[1,*]

[1]Department of Mechanical Engineering and Materials Science,
University of Pittsburgh, Pittsburgh, PA 15261, USA
[2]Jet Propulsion Laboratory, California Institute of Technology,
4800 Oak Grove Drive, Pasadena, CA 91109, USA

ABSTRACT

To ascertain the simultaneous thermal and electrical performance of a thermoelectric (TE) unicouple with interconnectors, a thermal-electric coupled iterative mathematical model is introduced. The non-linear constitutive equations describing TE phenomena within the unicouple are linked to a thermal resistance network describing the interconnectors' behavior. Thereupon, the thermal resistance of the interconnectors, and Joule heat generated within, are considered. Temperature dependent material properties are handled by integral-averaging techniques and an iterative solution methodology. Model form uncertainty is quantified by evaluating four unique analytic models. The first, the Implicit Thomson Model (ITM), considers the Thomson effect via integral averaging of the Seebeck coefficient. The second, the Explicit Thomson Model (ETM), decouples the Thomson effect from the Peltier effect; Thomson heat is explicitly solved using the Thomson coefficient. The third, the zT model, uses the figure of merit to describe the optimum efficiency-maximizing load resistance, and quantify device efficiency under maximum power scenarios. The last, the Differential Equation Model, does not assume distributions of Joule and Thomson heats to the cold- and hot-side interfaces as do the ITM, ETM and zT model. The predictive ability of each analytic model used within the unicouple-level model is compared to high-fidelity numeric results obtained from a three-dimensional, thermal-electric coupled model implemented in ANSYS CFX. Considering a range of hot-side unicouple temperatures, each analytic model exhibits agreement with one another, and with the numeric model. With increasing load resistance values, model form uncertainty and disagreement between analytic and numeric predictions decreases to a couple of percent at optimum operating points.

KEY WORDS: thermoelectric generator, thermal-electric coupled modeling, analytic and numeric modeling

1. INTRODUCTION

Thermoelectric devices (TEDs) are composed of specialized semiconductor materials and can convert a temperature gradient across said materials into an electrical potential; the inverse can also occur. Thermoelectric generators (TEGs) are comprised of multiple TEDs connected electrically in series, and are used to generate electrical power via the Seebeck effect [1]. While thermal conversion efficiency of TEGs is low, typically ranging between 4-8% [2], TEGs are advantageous in many design aspects that make them desirable energy conversion devices. Namely, they are small in size, have no moving parts, and have long operational lifetimes. Such properties make TEGs suitable for waste heat recovery in terrestrial applications

*Corresponding Matthew M. Barry: matthew.michael.barry@pitt.edu
DOI: http://dx.doi.org/10.1615/TFEC2022.aae.040927

[3–6]. TEGs are ideal for space systems such that electrical energy production can be achieved [7–11].

To design and evaluate the electrical and thermal performance of TEGs, various numerical models have been developed. Antonova and Looman [12] developed a thermal-electric finite element method model in ANSYS Workbench to predict the performance of TEDs by considering pertinent thermoelectric phenomena including the Seebeck, Peltier, and Thomson effects, as well as Joule heating. Chen et al. [13] developed a thermal-electric coupled numeric model in ANSYS Fluent using User Defined Functions to define the Joule, Peltier, and Thomson effects. These effects were applied to the energy equation as source terms, and the model's predictions were found to be in reasonable agreement with experimental data and results predicted by ANSYS. Björn et al. [14] developed a similar model in OpenFOAM and found the numeric results to match those predicted via a model in COMSOL, and the results of the model loosely matched values obtained via experimentation. Ledesma et al. [15] developed a fully-coupled thermal-electric finite volume method model in ANSYS CFX which included not only Joule heating and the Seebeck, Peltier, and Thomson effects, but also the Bridgman effect. The Bridgman effect is often neglected in numerical modeling of TEGs, but its inclusion reduced global energy imbalances by 47% at the the maximal hot-side temperature of the TEG. Though numerical models have been used to evaluate the performance of thermoelectric generators in lieu of experimental data, they are computationally intensive and there is variability of predicted results based on the inclusion and treatment of thermoelectric phenomena. Thus, robust analytic models are desirable for the rapid and accurate design and optimization of TEGs, such as in trade studies [16], where any compromise in fidelity is far out-weighed by reduced computational cost.

To understand the accuracy of various analytical modeling methods to predict the simultaneous thermal and electric behavior of a TED, it is important to understand the dependence of TEG performance on the material properties of the semiconducting materials. Semiconducting materials with a high Seebeck coefficient, low electrical resistivity, and low thermal conductivity are desirable due to their increased power densities and conversion efficiencies [17, 18]. Due to the temperature dependence of the aforementioned material properties, the accuracy of analytic modeling of TEGs is largely dependent on the method used to evaluate the material properties. Ioffe [19] suggested a constant properties model in which the material properties of semiconducting materials are assumed to be independent of temperature, and material properties are evaluated only at the average temperature across the TEG. Large error is associated with this method, in part due to neglecting of the Thomson effect under such assumptions. The Thomson effect is a manifestation of the temperature-dependence of the Seebeck effect, and is non-negligible when a moderate to large temperature difference occurs across the junctions. To more accurately model material properties, an integral average of the material properties can be used such that the temperature dependence of material properties is considered over a given temperature range [20]. Ponnusamy et al. [21] compared various averaging techniques to account for the temperature dependence of material properties, and found that a combination of integral averaging and spatial averaging of material properties was most physically appropriate, leading to an error of 1.5% in comparison to results found using a finite element method model implemented in ANSYS. Using integral-averaged material properties, various analytic models can be constructed to model the thermal and electrical behavior of these devices.

There exist four well-established analytic modeling methods. The first will be referred to as the Implicit Thomson Method (ITM), where the Thomson effect is implicitly incorporated into the formulation of heat input and output by using the integral-averaged Seebeck coefficient [22–24]. The second will be referred to as the Explicit Thomson Method (ETM), where the Thomson effect is explicitly defined in the formulation of heat input and output by separating the Thomson effect from the Peltier effect [25, 26]. The third is the figure of merit approach, which is predicated on maximizing the figure of merit of a material in order to maximize performance [22, 23]. The last model is derived from the thermoelectric general energy equation [27], and is referred to as the Differential Equation Model (DEM). The contribution of Joule heat is not assumed to be equally divided between the hot- and cold-junctions as is done in the ITM, ETM and zT model, nor is such an assumption made about the Thomson heat as done in the ETM. The DEM is re-derived in this work considering a TED functioning as a TEG with temperature-dependent material properties.

The existence of four unique analytic models, all with differing formative assumptions, causes uncertainty when constructing mathematical models of TEGs. The impetus of this work is to address the uncertainty associated with the selection of an analytic model. To this end, each analytic thermoelectric model is incorporated into a thermal-electric coupled mathematical model of a unicouple with interconnectors. Through the incorporation of interconnectors, the effect of their inherent thermal and electrical resistances, as well as the Joule heat generated, are considered when modeling the behavior of the thermoelectric materials. Each analytic model is evaluated over a range of thermal and electrical boundary conditions, and the unicouple performance is compared to a high-fidelity numeric results. It is demonstrated each analytic model is more than capable of predicting the simultaneous thermal-electric performance of the unicouple when incorporated into the novel mathematical model. It is also shown that model form uncertainty can be quantified when coincidently considering the predictions of all analytic models, and that the numeric results lie within the uncertainty of analytic predictions, indicating agreement between the modeling techniques.

2. MATHEMATICAL MODEL

Within the following, the DEM is derived for a TEG considering temperature dependent material properties, and all pertinent thermal-electric System Response Quantities (SRQs) are defined for the ITM, ETM, DEM and zT model. Following is the implementation of the analytic equations into a thermal-electric-coupled solution algorithm. To begin, a generic unicouple, as shown in Fig. 1 a), is the basis for the implementation of the novel mathematical model. The n- and p-type thermoelectric elements have a length of 10 [mm], and a cross-sectional area of 25 [mm^2]. The hot-side interconnector (HSI) has a length of 15 [mm], a thickness of 1 [mm] and a width of 5 [mm]. Each cold-side interconnector (CSI 1 and CSI 2) have a length of 7.5 [mm], a thickness of 1 [mm], and a width of 5 [mm]. The geometry of the unicouple used in the evaluation of the numeric and analytic models is not reflective of any proprietary, flight-qualified or proposed designs used by The National Aeronautics and Space Administration's (NASA) Jet Propulsion Laboratory (JPL) and/or their contractors. Rather, the geometry is generalized for demonstration of the models.

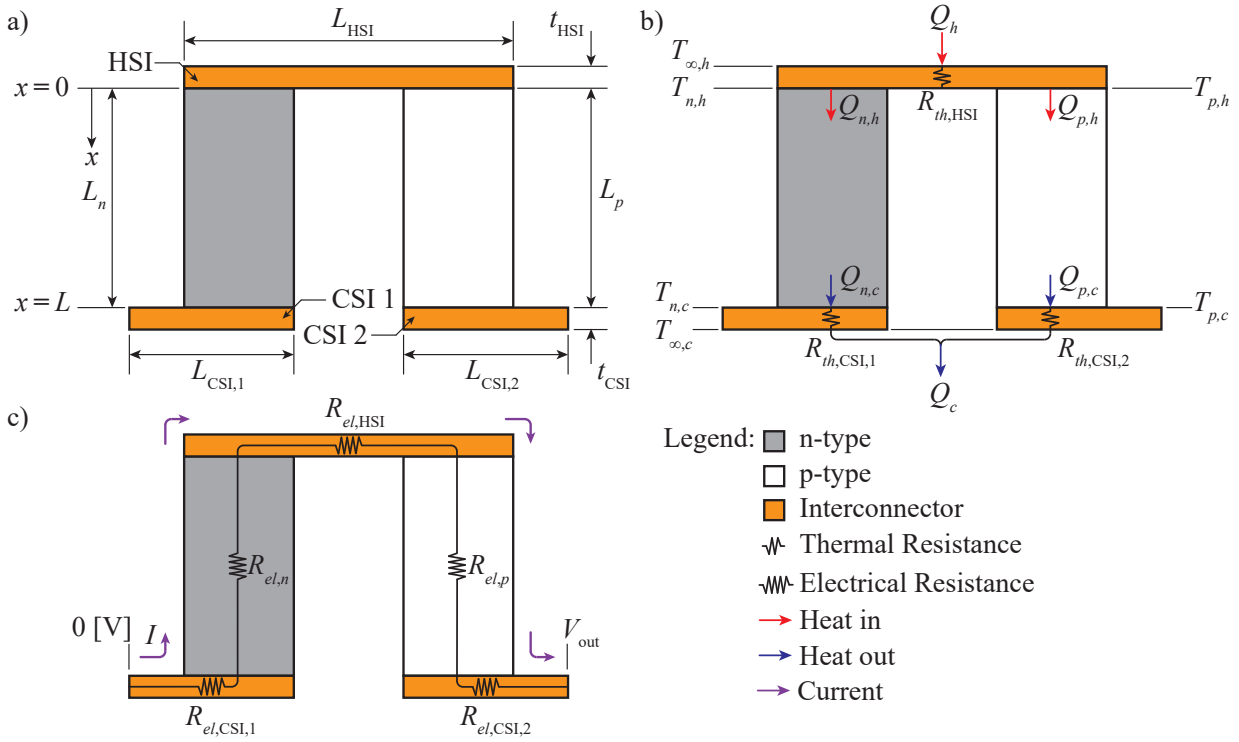

Fig. 1 Schematics of a) geometry of unicouple, b) interfacial temperatures, heat input and output and thermal resistances, and c) electrical boundary conditions, depiction of current and electrical resistances.

2.1 Differential Equation Model

Domenicali [28] outlined the phenomena occurring within thermoelectric materials, namely Joule, Peltier, Thomson, and Bridgman heating. These terms are cast into a general form which is expressed as

$$\nabla \cdot (\kappa \nabla T) + \rho \mathbf{J}^2 - T\mathbf{J} \cdot \left(\nabla \alpha \big|_T + \left(\frac{\partial \alpha}{\partial T} \right) \nabla T \right) - \alpha T \nabla \mathbf{J} = 0. \tag{1}$$

In order of appearance, the terms represent conduction, Joule, Peltier, Thomson, and Bridgman heat. To construct an analytic model, the general energy equation is considered in one-dimension: the axial, or x-direction. The Bridgman heat is neglected, for the current density vector $\mathbf{J}$ in one dimension is represented as a scalar value. The magnitude of $\mathbf{J}$ is expressed as the scalar value of current, I, per the cross-sectional area of the thermoelectric element leg, A. The Peltier effect is not included in the derivation of the one-dimensional representation of the general energy equation, for it occurs only at the interface of the thermoelectric material and interconnectors. The Peltier effect will be included when determining the heat into and out of the thermoelectric materials. To construct the DEM for a TEG, the general energy equation describing a thermoelectric element will be reduced to a solvable form. Thus, Eqn. 1, once multiplied by the cross-sectional area A, is represented in the axial direction as

$$\frac{\partial}{\partial x} \left(\kappa A \left(\frac{\partial T}{\partial x} \right) \right) + \frac{\rho I^2}{A} - TI \left(\frac{\partial \alpha}{\partial T} \right) \frac{\partial T}{\partial x} = 0. \tag{2}$$

It is noted, to simplify the analysis, specifically the third term of Eqn. 2, the Thomson coefficient, τ, is introduced, and is defined as

$$\tau = \left(\frac{\partial \alpha}{\partial T} \right) T. \tag{3}$$

To handle temperature-dependence of material properties, an integral-averaging technique is employed. The integral-averaged thermal conductivity, $\tilde{\kappa}$, electrical resistivity, $\tilde{\rho}$, Thomson coefficient, $\tilde{\tau}$, and Seebeck coefficient, $\tilde{\alpha}$, are defined as

$$\tilde{\kappa} = \frac{1}{(T_h - T_c)} \int_{T_c}^{T_h} \kappa(T)\, dT, \tag{4}$$

$$\tilde{\rho} = \frac{1}{(T_h - T_c)} \int_{T_c}^{T_h} \rho(T)\, dT, \tag{5}$$

$$\tilde{\tau} = \frac{1}{(T_h - T_c)} \int_{T_c}^{T_h} \tau(T)\, dT, \tag{6}$$

and

$$\tilde{\alpha} = \frac{1}{(T_h - T_c)} \int_{T_c}^{T_h} \alpha(T)\, dT. \tag{7}$$

Within Eqns. 4 through 7, T_h and T_c correspond to the hot- and cold-junction temperatures, as depicted in Fig. 1 b). The temperature-dependent properties of the n- and p-type materials are expressed as polynomials given in Tab. 2. It is noted that in Tab. 2, the materials used for the n- and p-type materials exist within

literature, and are not reflective of proprietary, flight-qualified or proposed materials used by NASA JPL and/or their contractors.

To solve Eqn. 2, it is recognized the solution $T(x)$ is a function of the summation of the homogeneous $T_H(x)$ and particular $T_P(x)$ solutions. To find the homogeneous solution, the right hand side of Eqn. 2 remains invariant. Thus, Eqn. 2 becomes a second-order, linear, ordinary differential equation. The solution to this equation is in the form $T_H(x)$=$e^{\lambda x}$, where λ represents the eigenvalue. Taking the first and second derivative of the assumed homogeneous solution yields

$$\frac{\partial T_H}{\partial x} = \lambda \exp(\lambda x), \tag{8}$$

and

$$\frac{\partial^2 T_H}{\partial x^2} = \lambda^2 \exp(\lambda x). \tag{9}$$

Substituting Eqns. 8 and 9 into the homogeneous form of Eqn. 2 results in

$$\exp(\lambda x)\left(\lambda^2 - \frac{\tilde{\tau}}{\tilde{\kappa}}\left(\frac{I}{A}\right)\lambda\right) = 0. \tag{10}$$

The quantity exp(λx) cannot equal zero, so the quantity within the parentheses must be equal to zero. The two solutions to λ are then

$$\lambda_{1,2} = \begin{cases} 0, \\ \dfrac{\tilde{\tau} I}{\tilde{\kappa} A}. \end{cases} \tag{11}$$

The homogeneous solution then takes the form

$$T_H(x) = c_1 \exp(\lambda_1 x) + c_2 \exp(\lambda_2 x) = c_1 + c_2 \exp\left(\frac{\tilde{\tau} I x}{\tilde{\kappa} A}\right). \tag{12}$$

To find the particular solution, the method of undetermined coefficients is used, where the solution $T_P(x)$ is assumed to have the form $c_3 x$. By substituting the first and second derivatives of $T_P(x)$ into Eqn. 2, the following results:

$$-\frac{\tilde{\tau} I}{\tilde{\kappa} A} c_3 = -\frac{\tilde{\rho}}{\tilde{\kappa}}\left(\frac{I}{A}\right)^2. \tag{13}$$

The particular solution is then in the form

$$T_P(x) = \frac{I x \tilde{\rho}}{\tilde{\tau} A}. \tag{14}$$

Combining the homogeneous solution, Eqn. 12, and the particular solution, Eqn. 14, the complete expression for the one-dimensional temperature distribution with a thermoelectric element with constant cross-sectional

area with the inclusion of Joule heat and the Thomson effect is expressed as

$$T(x) = c_1 + c_2 \exp\left(\frac{\tilde{\tau} I}{\tilde{\kappa} A} x\right) + \frac{I x \tilde{\rho}}{\tilde{\tau} A}. \tag{15}$$

Upon applying the aforementioned boundary conditions of $T(x = 0) = T_h$ and $T(x = L) = T_c$, as depicted in Fig. 1 a), the temperature profile within the leg can be expressed as

$$T(x) = T_h + \left(\frac{T_c - T_h - \frac{IL\tilde{\rho}}{\tilde{\tau} A}}{\exp\left(\frac{\tilde{\tau} IL}{\tilde{\kappa} A}\right) - 1}\right)\left(\exp\left(\frac{\tilde{\tau} I x}{\tilde{\kappa} A}\right) - 1\right) + \frac{I x \tilde{\rho}}{\tilde{\tau} A}. \tag{16}$$

To determine the heat into and out of the hot- and cold-side junctions, the derivative of the expression for the temperature distribution must be obtained and evaluated at the appropriate boundaries. Evaluating the derivative of temperature with respect to the spatial position x at the hot-side yields:

$$\left.\frac{dT}{dx}\right|_{x=L} = \left(\frac{T_c - T_h - \frac{IL\tilde{\rho}}{\tilde{\tau} A}}{\exp\left(\frac{I\tau L}{\tilde{\kappa} A}\right) - 1}\right)\left(\frac{I\tilde{\tau}}{\tilde{\kappa} A}\right)\exp\left(\frac{I\tilde{\tau} L}{\tilde{\kappa} A}\right) + \frac{I\tilde{\rho}}{\tilde{\tau} A}. \tag{17}$$

Similarly, evaluating the derivative of temperature with respect to the spatial position x at the cold-side yields the following:

$$\left.\frac{dT}{dx}\right|_{x=0} = \left(\frac{T_c - T_h - \frac{IL\tilde{\rho}}{\tilde{\tau} A}}{\exp\left(\frac{I\tilde{\tau} L}{\tilde{\kappa} A}\right) - 1}\right)\left(\frac{I\tilde{\tau}}{\tilde{\kappa} A}\right) + \frac{I\tilde{\rho}}{\tilde{\tau} A}. \tag{18}$$

The heat into the hot-side junction for a thermoelectric element, for all four analytic models, is expressed as:

$$Q_h = \begin{cases} \tilde{\alpha} I T_h - \dfrac{I^2 \tilde{R}_{el}}{2} + \tilde{K}(T_h - T_c) & \text{ITM and } zT \\ \alpha\big|_{T_h} I T_h + \tilde{K}(T_h - T_c) - \dfrac{I}{2}\left(I\tilde{R}_{el} + \tilde{\tau}(T_h - T_c)\right) & \text{ETM} \\ \alpha\big|_{T_h} I T_h - A\tilde{\kappa}\left.\dfrac{dT}{dx}\right|_{x=0} & \text{DEM.} \end{cases} \tag{19}$$

The heat exiting from the cold-side junction of a thermoelectric element, considering all four analytic models,

is given as:

$$Q_c = \begin{cases} \tilde{\alpha} I T_c + \dfrac{I^2 \tilde{R}_{el}}{2} + \tilde{K}(T_h - T_c) & \text{ITM and } zT \\ \alpha\big|_{T_c} I T_c + \tilde{K}(T_h - T_c) + \dfrac{I}{2}\left(I\tilde{R}_{el} + \tilde{\tau}(T_h - T_c) \right) & \text{ETM} \\ \alpha\big|_{T_c} I T_c - A\tilde{\kappa} \dfrac{dT}{dx}\Big|_{x=L} & \text{DEM.} \end{cases} \tag{20}$$

In Eqns. 19 and 20, is it noted the Seebeck coefficient α is not integral-averaged when considering the ETM and DEM, but evaluated at the respective interfacial temperature. It is further noted that previous authors [26] have taken a similar approach to constructing an expression for heat input and output of a thermoelectric element by resolving the thermoelectric general energy equation, however, their solution considered the integral-averaged Seebeck coefficient in addition to an explicit Thomson heating contribution. To solve Eqns. 19 and 20, the electric current I must be resolved. The electric current is expressed as:

$$I = \begin{cases} \dfrac{V_{oc}}{R_{int} + R_{load}} & \text{ITM, ETM, DEM and } zT \max(P_{out}) \\ \dfrac{V_{oc}}{R_{int}(m_{opt} + 1)} & zT \max(\eta). \end{cases} \tag{21}$$

Within Eqn. 21, V_{oc} is the open-circuit voltage, commonly referred to as the Seebeck voltage when an external electrical load is applied, R_{int} is the internal resistance of the unicouple, considering not only the thermoelectric materials, but interconnectors, and R_{load} is the externally applied load resistance. The Seebeck voltage is calculated via the summation of the integral-averaged Seebeck coefficients of the n- and p-type materials evaluated between the hot- and cold-side boundary junction temperatures such that

$$V_{oc} = \tilde{\alpha}_n(T_{n,h} - T_{n,c}) + \tilde{\alpha}_p(T_{p,h} - T_{p,c}). \tag{22}$$

The internal electrical resistance is calculated via the summation of the electrical resistances of the n- and p-type materials, plus that of the interconnectors, evaluated in the direction of the flow of current as shown in Fig. 1 c), such that

$$R_{int} = \tilde{R}_{el,n} + \tilde{R}_{el,p} + \tilde{R}_{el,\text{HSI}} + \tilde{R}_{el,\text{CSI 1}} + \tilde{R}_{el,\text{CSI 2}}. \tag{23}$$

Within Eqn. 23, the n- and p-type electrical resistances, as well as that of the hot- and cold-side interconnectors, are generally expressed as

$$\tilde{R}_{el} = \frac{\tilde{\rho} L}{A(T_h - T_c)} = \frac{L}{A(T_h - T_c)} \int_{T_c}^{T_h} \rho(T)\, dT \tag{24}$$

where L is the length and A is the cross-sectional area of the element that the current travels along and through, respectively, and $\tilde{\rho}$ is the integral-averaged electrical resistivity. The load resistance, R_{load} in Eqn. 21 is a varied to determine the point of maximum power and point of maximum efficiency. The variable m_{opt} in Eqn. 21 is a multiplier applied to the internal resistance that maximizes efficiency when considering the zT model, such that $R_{load} = R_{int} m_{opt}$ can be used in the first expression of Eqn. 21, or used in second

expression of Eqn. 21 as is, and can be defined as

$$m_{opt} = (1 + zT_{avg})^{1/2}. \tag{25}$$

Within Eqn. 25, z is the figure of merit of the thermoelectric materials, which is defined as

$$z = \frac{(|\tilde{\alpha}_n| + |\tilde{\alpha}_p|)^2}{((\tilde{\rho}_n\tilde{\lambda}_n)^{1/2} + (\tilde{\rho}_p\tilde{\lambda}_p)^{1/2})^2}, \tag{26}$$

where T_{avg} is the arithmetic average temperature of the hot- and cold-side junction temperature. With the definition of Eqns. 22 through 26, and the specification of R_{load}, Eqn. 21 can be resolved, and the heat into and out of the junctions can be determined, for each of the four analytic models. Only one term remains for the determination of the main SRQs of interest, namely power output and conversion efficiency. That term is the electric potential developed across the terminals of the unicouple, expressed through the non-Ohmic voltage-current relation [29]. The output voltage is expressed as

$$V_{out} = V_{oc} - IR_{int}. \tag{27}$$

The electrical power output is then defined as

$$P_{out} = I^2R_{load} = Q_h - Q_c = IV_{out}. \tag{28}$$

Within Eqn. 28, the second term is the electrical power output as described by the Maximum Power Transfer Theorem [30], the third is the thermodynamic definition of power for a heat engine, and the fourth being the definition electrical power. Given the electrical power output and heat input, the thermal conversion efficiency is defined as

$$\eta = \begin{cases} \dfrac{P_{out}}{Q_h} & \text{ITM, ETM, DEM and } zT \text{ max}(\eta) \\ \dfrac{z(T_h - T_c)}{4} - \dfrac{T_h - T_c}{2T_h} + 2 & zT \text{ max}(P_{out}). \end{cases} \tag{29}$$

2.2 Thermal Resistance Network

To include Joule heating within the HSI and CSIs, as well as determine the n- and p-type hot- and cold-side interfacial temperatures, the aforementioned constitutive analytic models were integrated into a thermal resistance network, as depicted in Fig. 1 b). The heat entering the unicouple, Q_h, is expressed as

$$Q_h = \frac{T_{\infty,h} - T_h}{R_{th,\text{HSI}}}, \tag{30}$$

where the thermal resistance of the HSI is expressed as

$$R_{th,\text{HSI}} = \frac{t_{\text{HSI}}}{\kappa_{\text{HSI}}A_{\text{HSI}}}. \tag{31}$$

Within Eqn. 31, t_{HSI} is the thickness of the HSI, κ_{HSI} is the thermal conductivity of the HSI, and A_{HSI} is the cross-sectional flow area of heat for the HSI. By employing an energy balance to the HSI, the heat entering the unicouple must be equal to the heat generated by Joule heating ($I^2 R_{el,\text{HSI}}$) in the HSI plus the heat entering both the n- and p-type materials, denoted as $Q_{n,h}$ and $Q_{p,h}$ respectively, as described by Eqn. 19. Similarly, by employing an energy balance to the CSIs, the heat existing the n- and p-type materials, denoted as $Q_{n,c}$ and $Q_{p,c}$ respectively and as describe by Eqn. 20, summed with the that generated by Joule heating in each CSI ($I^2 R_{el,\text{CSI 1}}$ and $I^2 R_{el,\text{CSI 2}}$), must be equal to the heat exiting the unicouple. The heat exiting the unicouple is denoted as Q_c and is expressed as

$$Q_c = \frac{T_c - T_{\infty,c}}{R_{th,\text{CSI}}}, \tag{32}$$

where the thermal resistance of the CSI is expressed as

$$R_{th,\text{CSI}} = \frac{t_{\text{CSI}}}{\kappa_{\text{CSI}} A_{\text{CSI}}}. \tag{33}$$

Within Eqn. 33, t_{CSI} is the thickness of the CSI, κ_{CSI} is the thermal conductivity of the CSI, and A_{CSI} is the cross-sectional flow area of heat for the CSI. With the specification of Dirichlet boundary conditions, namely $T_{\infty,h}$ and $T_{\infty,c}$, the interfacial temperatures T_h and T_c, which provide bounds to the heat equations (Eqn. 19 and Eqn. 20), can be resolved. Additionally, quantification of heat into and out of the unicouple as expressed by Eqns. 30 and 32, can be determined.

2.3 Solution Methodology

A fully-coupled thermal-electric iterative solution algorithm was implemented to simultaneously resolve the thermal and electric behavior of a unicouple. To do such, Eqns. 19, 20, 30 and 32 were cast in terms of the interfacial temperatures $T_{n,h}$ and $T_{p,h}$ (i.e. T_h), and $T_{n,c}$ and $T_{p,c}$ (i.e. T_c). Given an initial value of current, initialized temperature values, and a specified load resistance, all material properties defined by Eqns. 4-7 were defined. With updated material properties, all values for electrical resistance of the n- and p-type materials, as well as the HSI and CSIs as defined by Eqn. 24, were populated. This allowed for the calculation of the total device electrical resistance as defined by Eqn. 23. The simultaneous system of equations for temperature was then resolved. Based upon newly updated temperatures, the electrical response quantities, namely V_{oc} and I defined by Eqns. 22 and 21 respectively, were defined. Additionally, the heat entering the unicouple as defined by Eqn. 30, that into the n- and p-type materials as defined by Eqn. 19, that out of the n- and p-type materials as defined by Eqns. 20, and that leaving the unicouple as defined by Eqn. 32, were evaluated. This process was repeated, using the newly solved for values of I and interfacial temperatures as initial values to the aforementioned system of equations, until convergence was reached.

The criteria for convergence is as follows. The maximum absolute error between successive iterations for all SRQs was set to a value of 1E-10. These SRQs include interfacial temperatures, heats, Seebeck and Ohmic voltages, total unicouple electrical resistance and current. Additionally, from the continuity of heat equations describing the heat entering and exiting the hot- and cold-side junctions were cast such that a residual, or imbalance of heats, was defined. The residual criteria for the conservation equations was set to a value of 1E-12. Convergence was achieved when both the error and residual criteria were met.

2.4 Model Validation

To determine the validity of the proposed mathematical model, an implicit, fully-coupled, three-dimensional finite volume method model was implemented in ANSYS CFX. All pertinent thermoelectric phenomena were coupled to the energy equation via volumetric or surface source terms expressed using CFX's Expression

Language. Using the Electromagnetics model, which allowed the application of the Electric Field model, the electric field and current density vector were resolved, allowing for the resolution of the Bridgman heat. Joule heating was intrinsically accounted for with the resolution of the electric current density. Details of the model construction and implementation can be found in [31]. It is noted the ANSYS CFX model used herein was dually validated to ANSYS Thermal-Electric [12] and ANSYS Fluent [13] within the work of Wielgosz et al. [31], and exhibited excellent agreement in thermal and electrical predictions. Furthermore, it is reiterated that ANSYS Thermal-Electric and ANSYS Fluent have both been demonstrated to yield agreement with experimental data.

3. RESULTS AND DISCUSSION

Within the following sections, a rigorous comparison of the mathematical model results to those predicted by a fully-coupled thermal-electric finite volume method model are presented. After it is established that the analytic models are faithfully able to predict the thermal and electric performance at conditions of maximum power and maximum thermal conversion efficiency, the effect of hot-side temperature and load resistance are independently studied. The ability of the proposed analytic model, as well as existing analytic models, implemented within a unicouple-level mathematical model is evaluated for these varying conditions. As will be seen, the proposed DEM model yields performance predictions comparable to the ITM, ETM and zT models. With the introduction of the DEM model, a more robust average analytic value can be obtained considering all aforementioned models, and a better-defined confidence interval can be generated around the average analytic result.

3.1 Model Comparison to Numeric

Before a sweep of hot-side temperatures and load resistances was conducted, the ability of each analytic model integrated within the unicouple-level mathematical model to predict not only the electrical, but also thermal behavior, was determined. Each model was compared to the results generated by ANSYS CFX for the highest hot-side temperature and under two situations of load resistance; one in which power output was maximized ($R_{load} = R_{int}$ for ITM, ETM, DEM and where zT was maximizing power output), and one in which thermal efficiency was maximized. The comparison between the models are shown in Tab. 1.

Table 1 Comparison of mathematical models to ANSYS CFX with $T_{\infty,c} = 300$ K, $T_{\infty,h} = 650$ K, solving for maximum power output and maximum efficiency, with the average value of the all four mathematical models and the model form uncertainty [32] reported. Percent differences taken with respect to numeric results.

	Maximum Power										
SRQ	CFX	ITM	|% Diff.|	ETM	|% Diff.|	DEM	|% Diff.|	zT	|% Diff.|	Avg.	U [%]
Q_h [W]	3.82207	3.79373	0.74	3.87660	1.42	3.89165	1.80	3.79373	0.74	3.83893	2.68
Q_c [W]	3.50157	3.46939	0.92	3.55228	1.44	3.56732	1.86	3.46939	0.92	3.51460	2.93
V_{oc} [dV]	1.12027	1.12480	0.40	1.12478	0.40	1.12478	0.40	1.12480	0.40	1.12479	2.01e-3
R_{int} [mΩ]	9.77717	9.85103	0.75	9.85102	0.75	9.85101	0.75	9.85103	0.75	9.85102	1.90e-4
I [A]	5.72902	5.70905	0.35	5.70898	0.35	5.70896	0.35	5.70905	0.35	5.70901	1.61e-3
P_{out} [dW]	3.20494	3.21077	0.18	3.21069	0.18	3.21067	0.18	3.21077	0.18	3.21073	3.21e-3
η [%]	8.38535	8.46337	0.93	8.28221	1.24	8.25016	1.63	8.57711	2.26	8.39321	3.61
	Maximum Efficiency										
SRQ	CFX	ITM	|% Diff.|	ETM	|% Diff.|	DEM	|% Diff.|	zT	|% Diff.|	Avg.	U [%]
Q_h [W]	3.71209	3.69137	0.56	3.75571	1.17	3.76216	1.34	3.68280	0.79	3.72301	2.20
Q_c [W]	3.39129	3.37191	0.57	3.43701	1.34	3.44385	1.54	3.36411	0.80	3.40422	2.42
V_{oc} [dV]	1.12081	1.12482	0.36	1.12481	0.36	1.12481	0.36	1.12482	0.36	1.12482	1.01e-3
R_{int} [mΩ]	9.73032	9.85105	1.23	9.85104	1.23	9.85104	1.23	9.85105	1.23	9.85105	1.15e-4
I [A]	5.02164	5.05726	0.71	5.00532	0.33	4.97941	0.84	5.00380	0.36	5.01145	1.28
P_{out} [dW]	3.17462	3.16901	0.18	3.16201	0.40	3.15835	0.51	3.16187	0.40	3.16281	0.28
η [%]	8.55211	8.65420	1.19	8.48593	0.78	8.46096	1.07	8.65351	1.18	8.56365	2.40

As seen within Tab. 1, all analytic models incorporated into a unicouple-level mathematical model are able to accurately predict not only the thermal performance, namely heat input and output, but also the electrical performance for situations of maximum power and maximum efficiency. The ITM and zT model consistently have more accurate predictions of heat input and output under both load resistance situations considered, but the predictions are less than those obtained via CFX. These models provide a more conservative estimate of performance. The ETM and DEM both over-predict heat into and out of the unicouple for situations of maximum power and maximum efficiency. It is further seen that the numeric result falls within the 95% confidence interval around the average value of the the mathematical models.

All analytic models are able to accurately predict the electrical performance of the unicouple. Considering the Seebeck voltage predictions, the maximum percent difference is less than half a percent for situations where power output and thermal conversion efficiency are maximized. Similarly the analytic models accurately predict the generated current under situations where power output is maximized, with the ETM and zT model having the lowest difference in comparison to numeric when the thermal conversion efficiency is maximized. All analytic model predictions of generated electric current have percent differences below one percent, in part due to the low percent differences of calculated Seebeck voltage and internal resistances. The analytic models predict power output with percent differences at or below 0.51% considering both operating points.

The ITM, followed by the ETM, DEM and zT model exhibit the closest agreement with CFX when predicting thermal conversion efficiency when maximizing power output, with percent differences increasing from less than 1% to over 2.20%. When considering maximum efficiency, the ETM followed by the DEM, zT model and then ITM had the closest predictions, with all percent differences below 1.2%. Although there are situations where the percent differences are perceived to be large in comparison to the numeric data, it is noted the obtained values for most SRQs via the high-fidelity numeric model lie within the 95% confidence interval around the average value of the four unique mathematical models. The slight discrepancies in V_{oc}, I, R_{int} and P_{out} are attributed to the localized Bridgman heating at the interior corners of the hot-side junction and exterior corners of the cold-side junctions; regions where the gradient of the current density is highest. With this localized heating, the average interfacial temperatures will show some disagreement with the simplified mathematical model. Nevertheless, the percent differences associated with the aforementioned SRQ values are universally less than one and a quarter percent.

3.2 Temperature Sweep

The thermal and electrical performance of all analytic models, i.e. the pre-existing ITM, ETM, and zT analytic model, as well as the DEM presented herein, were evaluated for hot-side temperatures ranging from 350 to 650 [K] in 50 [K] increments with an invariant cold-side temperature of 300 [K]. Models were evaluated at a maximum power configuration. Thermal and electrical performance of each analytical model was compared to numeric results. In terms of thermal performance, it is seen in Figs. 2 a) and b) that the ETM and DEM overestimate both heat input and heat output at increased values of hot-side temperature in comparison to the ITM, zT model and CFX's predictions. As seen in Tab. 1, the percent differences between the ETM and DEM models for heat input and output on the order of 1-2%. Conversely, the ITM and zT model produce conservative estimates of heat input and output as hot-side temperature increases. It is noted the heat input near-linearly increases with hot-side temperature, whereas heat output exhibits a slight monotonic decrement with increasing hot-side temperature.

In addition to thermal performance predictions, it is necessary to compare electrical performance predictions. It is seen in Figs. 3 a) and b) that all analytic models result in current and voltage output predictions that remain in close agreement with numeric results, and one another, over the range of hot-side temperatures. The ITM, ETM, DEM and and zT model all have percent differences of 0.35% for current and output voltage predictions in comparison to CFX. Additionally, the ETM, ITM, DEM and zT model all accurately predict power output as seen in Fig. 4 a). While the ETM and DEM slightly overestimate heat input and output, they provide conservative estimates of thermal efficiency, as seen in Fig. 4 b). Both the ITM and zT model over-predict efficiency.

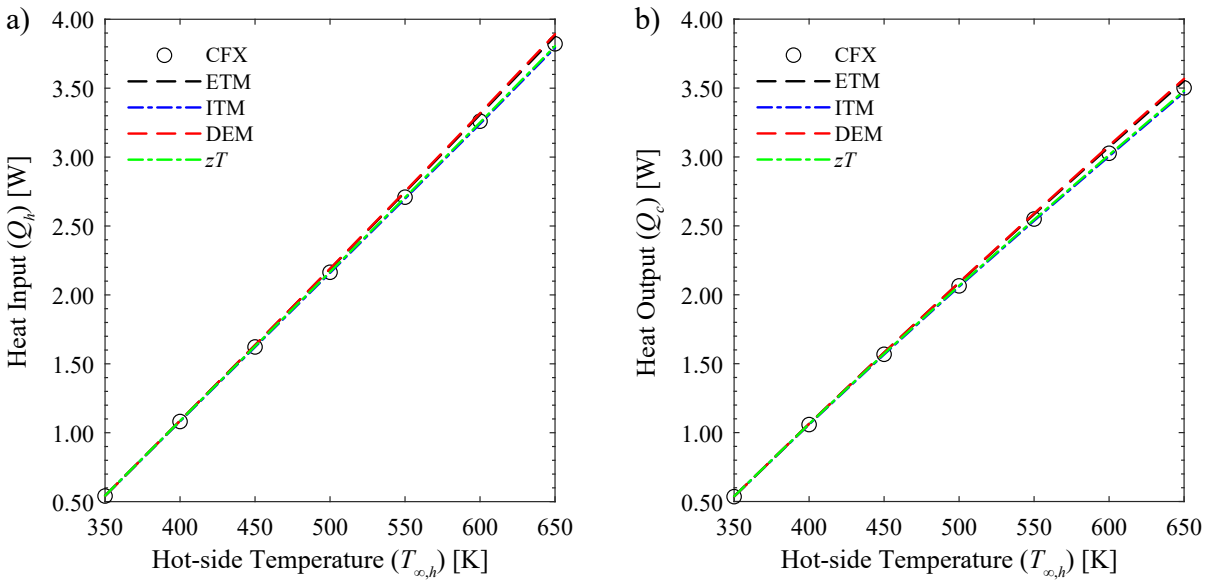

Fig. 2 a) Heat input and b) heat output over a range of hot-side temperatures for all models.

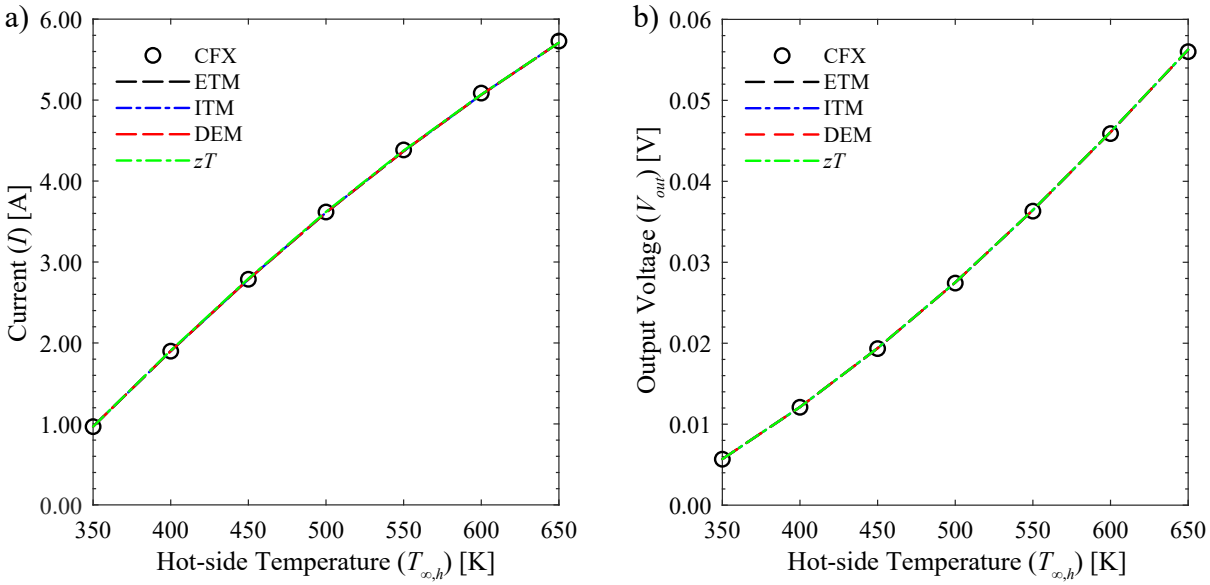

Fig. 3 a) Current and b) output voltage via each analytic model over a range of hot-side temperatures in comparison to numeric.

3.3 Load Resistance Sweep

The thermal and electrical performance of each analytic model implemented into the unicouple-level mathematical model, as well as the numeric model, was additionally evaluated over a range of load resistances. The cold- and hot-side temperatures was kept invariant at 300 [K] and 650 [K], respectively, while load resistance varied between 1E-5 and 1E3 [Ω]. As opposed to the previously described hot-side temperature sweep, where analytic models were individually compared to each other and to the numeric model, the results will be presented as follows—using the unique mathematical models, the average and standard deviation of every SRQ of interest is quantified at each value of load resistance such that the model form uncertainty can be quantified in terms of a 95% confidence interval around the average analytic result.

As seen in Fig. 5 a), mathematical modeling methods over-predict current and have highest uncertainty at low

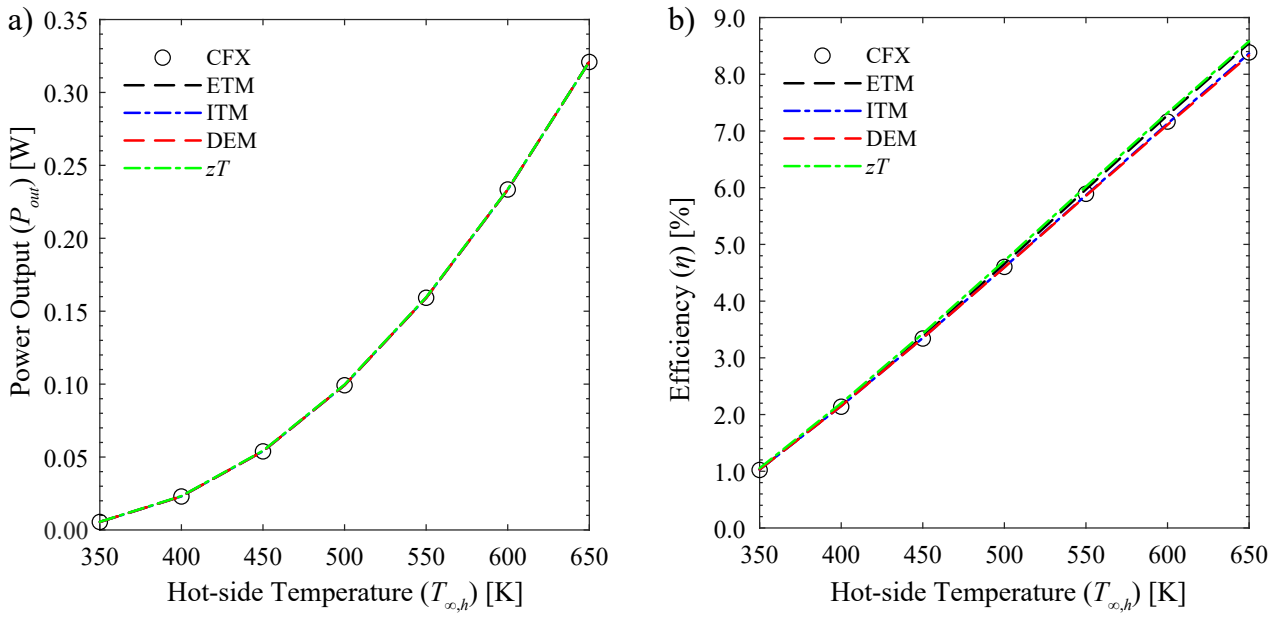

Fig. 4 a) Power output and b) efficiency over a range of hot-side temperatures for all models.

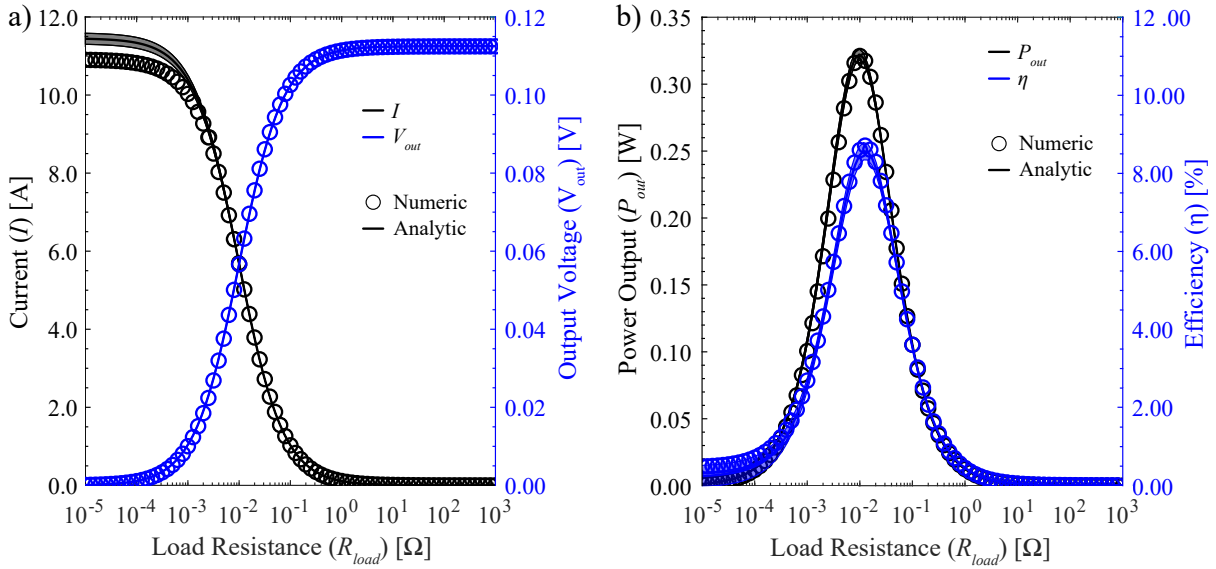

Fig. 5 a) Current and output voltage, and b) power out and efficiency predictions of the averaged-results of the analytic models in comparison to predictions via ANSYS CFX over a range of load resistance values.

values of load resistance. This is attributed to the omission of the Bridgman heat within analytic models, which is non-trivial at low load resistance to internal resistance ratios [31]. The over-prediction of current is not of concern because the point of maximum power output and thermal efficiency occur at approximately 9.8E-3 and 11.8E-3 [Ω], respectively, as shown in Fig. 5 b). At these power output and efficiency maximizing values of load resistance, where TEGs are typically designed to operate, current predicted by analytic modeling methods remains in close agreement with numeric results. Although the analytic models on average over-predict current at low load resistance values, the predicted output voltage is in agreement with the numeric model. It can also be seen in Fig. 5 b) that power output and thermal efficiency are accurately predicted by mathematical modeling methods in comparison to numeric results. With increasing load resistance values, produced electric current tends to zero whereas the output voltage increases to a maximum; there is also great agreement with mathematical and numeric predictions.

As shown in Fig. 6, mathematical modeling methods over-predict heat input and output and have the highest uncertainty at decreased values of load resistance. Once again, the TEG would not operate at such low values of load resistance, where neither efficiency nor power is maximized, and thus although the numeric predictions are within the confidence interval of the analytic predictions, it would be inadvisable to design around these operating points. This over-prediction of heat input and output at low load resistances is attributed to the high current values. At high current density values, the Bridgman heat is non-negligible, and the analytic models are unable to quantify this phenomena. The omission of Bridgman heat results in an order of magnitude increase in the global energy imbalance when compared to models incorporating the Bridgman heat [31], thus a discrepancy between numeric and mathematical models is expected in this region. As the load resistance increases from the minimum to values where the device is operating at maximum power and maximum efficiency, the average heat input and output predictions of the mathematical models match the numeric predictions. With a further increase in load resistance, all analytic and numeric values converge, for the produced electric current tends to zero, and conduction dominates behavior.

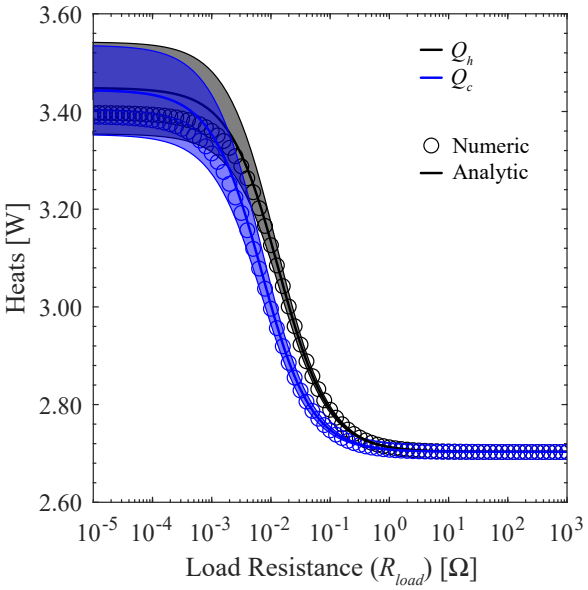

Fig. 6 Heat input and output predictions of the averaged-results of the analytic models in comparison to predictions via ANSYS CFX over a range of load resistance values.

From Figs. 5 and 6, it is seen that mathematical modeling methods are able to accurately predict the thermal and electric behavior of a unicouple over the range of desired operating points. The temperature-dependent DEM is able to accurately predict the power output and thermal conversion efficiency at points of maximum power and maximum thermal conversion efficiency, with the same level of accuracy as the existing ITM, ETM and zT models. At low load resistance values, on the order of 3e-3 [Ω] , the mathematical models' predictions of the produced electrical current (Fig. 5 a)), and subsequent heat input and output (Fig. 6) deviate from the high-fidelity numeric results. But, as seen from Fig. 5 b), the power output and efficiency values are sub-optimal at or below the low resistance where marked deviation is witnessed, and the device should not be operated under said conditions. Additionally, it can be seen that the iterative mathematical models are as capable as the three-dimensional finite volume method model in predicting both the simultaneous electrical and thermal performance of a TEG. Thus, with proper consideration of material properties and modeling approaches, the aforementioned mathematical models are sufficient for device design and optimization, and can be used independently of numeric models. The use of either the ITM, ETM, DEM or zT model is incontrovertible. The construction and use of numeric models still serve a purpose of validating analytic models, but are not required to resolve the thermal-electric behavior of a TEG.

4. CONCLUSION

Four unique constitutive analytic models describing the behaviour of thermoelectric elements—the Implicit Thomson Model (ITM), Explicit Thomson Model (ETM), Differential Equation Model (DEM), and zT model—were integrated into mathematical model of a thermoelectric unicouple. Using a thermal resistance network and an iterative solution methodology, the effect of the interconnectors and the use of temperature-dependent materials was able to be considered and handled, respectively. In doing such, a thermal-electric coupled, unicouple-level mathematical model was created. Each of the constitutive analytic

models incorporated into the mathematical model were evaluated at conditions that maximized power output and thermal conversion efficiency, and were shown to be in good agreement with results generated via a high-fidelity, three-dimensional thermal-electric coupled model implemented in ANSYS CFX. This was evidenced by low percent differences between the mathematical and numerical results. It was found the ITM, ETM, DEM and zT model are all capable of accurately predicting device performance at conditions of maximum power output and maximum thermal conversion efficiency. The mathematical model, separately considering all four constitutive equations, was then evaluated over a range of hot-side temperatures when considering a situation of maximum power output, and was shown to be in good agreement with numeric results. The ETM and DEM over-predict heat input, and consequently under-predict thermal conversion efficiency. The opposite is seen with the ITM and zT model. All models had accurate predictions of electrical behaviour, namely open-circuit voltage, current and power output.

In addition to providing accurate performance predictions of a TEG, the introduction of the novel mathematical model, considering all four analytic formulations of the thermoelectric effects within, allows for robust model form uncertainty quantification. As the load resistance was varied, agreement and disagreement between the mathematical and numerical models was observed. In regions of low load resistance values, the greatest deviation between mathematical and numerical results was seen; the mathematical model's average value had an over-prediction of current and heat input and output. With increasing load resistance values nearing the region where power output and thermal conversion efficiency were maximized, agreement between modeling techniques was observed. Furthermore, the numeric values lied within the confidence interval around the mathematical model's average value for power output and thermal conversion efficiency, indicating further agreement between the two techniques. Thus, all aforementioned constitutive models, when integrated into a unicouple-level mathematical model, are able to accurately quantify the simultaneous thermal-electric performance of a thermoelectric generator.

ACKNOWLEDGMENTS

This research was carried out at the Jet Propulsion Laboratory, California Institute of Technology, under a contract with the National Aeronautics and Space Administration, CL#: 21-5717, and at the University of Pittsburgh. Computational resources and support were provided by the Center for Research Computing (CRC) at the University of Pittsburgh.

The remainder of this page has been intentionally left blank.

Table 2 Polynomial expressions for temperature dependent thermoelectric and interconnector properties.

n-type $Bi_2Te_{1.9}Se_{1.1}$ [33]		p-type $Ge_{0.7}Pb_{0.13}Te$+3% Bi_2Te_3 [34]	
α_N	= (-3.202118465009907e-19)T^6 + (9.203585371307136e-16)T^5 + (-1.073152310161369e-12)T^4 + (6.493910899794523e-10)T^3 + (-2.15109875689092e-7)T^2 + (3.646981516744837e-5)T + (-0.002561458547361978)	α_P	= (-1.500813826446285e-19)T^6 + (4.293338680148655e-16)T^5 + (-5.014714714245148e-13)T^4 + (3.042590912073281e-10)T^3 + (-1.010501330398025e-7)T^2 + (1.822883155906853e-5)T + (-0.001365897370156843)
κ_N	= (3.634218867237926e-15)T^6 + (-1.119227631273517e-11)T^5 + (1.410461035072385e-8)T^4 + (-9.307231318913803e-6)T^3 + (0.003396895991439032)T^2 + (-0.6552982139209359)T + (54.70633936832369)	κ_P	= (5.238086549608868e-17)T^6 + (-2.927636770231909e-13)T^5 + (5.844390241944433e-10)T^4 + (-5.642804450717544e-7)T^3 + (0.0002909446395983974)T^2 + (-0.08063418038142083)T + (11.00293123390308)
σ_N	= (-3.253703447464733e-8)T^5 + (8.721294302777075e-5)T^4 + (-0.09344706416614766)T^3 + (50.97626108178136)T^2 + (-14667.25239632805)T + (1892814.656277739)	σ_P	= (1.319288092705862e-10)T^6 + (-3.85669843140294e-7)T^5 + (0.0004638862454473422)T^4 + (-0.297110247163325)T^3 + (109.4552349385509)T^2 + (-22997.10238999909)T + (2309068.907784006)
Interconnectors - Copper			
κ_{int}	= 401		
σ_{int}	= 6E7		

The remainder of this page has been intentionally left blank.

NOMENCLATURE

Variables

A	area	(m^2)	P_o	power output	(W)
I	current	(A)	Q	heat	(W)
J	current density vector	(Am^{-2})	R	resistance, electrical or thermal	(Ω or KW^{-1})
K	thermal conductance	(WK^{-1})	T	thickness	(m)
m	ratio of resistances (-)		T	temperature	(K)
L	Length	(m)	U	uncertainty (%)	
N	n-type	(-)	V	voltage	(V)
P	p-type	(-)	zT	dimensionless figure of merit	(-)

Subscripts and Superscripts

c	cold-side	N	n-type
el	electrical	oc	Seebeck
h	hot-side	opt	optimum
int	internal	out	output
∞	free-stream	P	p-type
$load$	load	th	thermal

Greek Letters

α	Seebeck coefficient	(VK^{-1})	ρ	electrical resistivity	(Ωm)
η	thermal conversion efficiency	(-)	σ	electrical conductivity	(Sm^{-1})
κ	thermal conductivity	($Wm^{-1}K^{-1}$)	τ	Thomson coefficient	(VK^{-1})
λ	eigenvalue	(-)			

Acronyms

CSI	cold-side interconnector	ITM	Implict Thomson Model
DEM	Differential Equation Model	SRQ	system response quantity
ETM	Explicit Thomson Model	TE	Thermoelectric
FVM	finite volume method	TED	thermoelectric device
GEQ	general energy equation	TEG	thermoelectric generator
HSI	hot-side interconnector	TRN	thermal resistance network

REFERENCES

[1] T. J. Seebeck, "Ueber die magnetische polarisation der metalle und erze durch temperaturdifferenz," *Annalen der Physik*, vol. 82, no. 3, pp. 253–286, 1826.

[2] Y. Wu, J. Yang, S. Chen, and L. Zuo, "Thermo-element geometry optimization for high thermoelectric efficiency," *Energy*, vol. 147, pp. 672–680, 2018.

[3] T. Hendricks and W. T. Choate, "Engineering scoping study of thermoelectric generator systems for industrial waste heat recovery," tech. rep., Pacific Northwest National Lab.(PNNL), Richland, WA (United States), 2006.

[4] X. Gou, S. Yang, H. Xiao, and Q. Ou, "A dynamic model for thermoelectric generator applied in waste heat recovery," *Energy*, vol. 52, pp. 201–209, 2013.

[5] T. Wang, W. Luan, W. Wang, and S.-T. Tu, "Waste heat recovery through plate heat exchanger based thermoelectric generator system," *Applied Energy*, vol. 136, pp. 860–865, 2014.

[6] S. Lan, Z. Yang, R. Chen, and R. Stobart, "A dynamic model for thermoelectric generator applied to vehicle waste heat recovery," *Applied energy*, vol. 210, pp. 327–338, 2018.

[7] F. Ritz and C. E. Peterson, "Multi-mission radioisotope thermoelectric generator (mmrtg) program overview," in *2004 IEEE*

Aerospace Conference Proceedings (IEEE Cat. No. 04TH8720), vol. 5, pp. 2950–2957, IEEE, 2004.

[8] G. Bennett, J. Lombardo, R. Hemler, G. Silverman, C. Whitmore, W. Amos, E. Johnson, A. Schock, R. Zocher, T. Keenan, *et al.*, "Mission of daring: the general-purpose heat source radioisotope thermoelectric generator," in *4th international energy conversion engineering conference and exhibit (IECEC)*, p. 4096, 2006.

[9] J. Yang and T. Caillat, "Thermoelectric materials for space and automotive power generation," *MRS bulletin*, vol. 31, no. 3, pp. 224–229, 2006.

[10] R. O'Brien, R. Ambrosi, N. Bannister, S. Howe, and H. V. Atkinson, "Safe radioisotope thermoelectric generators and heat sources for space applications," *Journal of Nuclear Materials*, vol. 377, no. 3, pp. 506–521, 2008.

[11] T. C. Holgate, R. Bennett, T. Hammel, T. Caillat, S. Keyser, and B. Sievers, "Increasing the efficiency of the multi-mission radioisotope thermoelectric generator," *Journal of Electronic Materials*, vol. 44, no. 6, pp. 1814–1821, 2015.

[12] E. E. Antonova and D. C. Looman, "Finite elements for thermoelectric device analysis in ansys," in *ICT 2005. 24th International Conference on Thermoelectrics, 2005.*, pp. 215–218, IEEE, 2005.

[13] M. Chen, L. A. Rosendahl, and T. Condra, "A three-dimensional numerical model of thermoelectric generators in fluid power systems," *International Journal of Heat and Mass Transfer*, vol. 54, no. 1-3, pp. 345–355, 2011.

[14] B. Pfeiffelmann, A. C. Benim, and F. Joos, "A finite volume analysis of thermoelectric generators," *Heat Transfer Engineering*, vol. 40, no. 17-18, pp. 1442–1450, 2019.

[15] E. M. Ledesma, S. Sammak, and M. Barry, "Modeling bridgman heating in thermoelectric generators," in *ASTFE Digital Library*, pp. 259–268, Begel House Inc., 2021.

[16] M. Durka, J.-P. Fleurial, S. Wielgosz, S. Rile, M. Barry, D. Woerner, B. Barstow, F. Drymiotis, and B. Nesmith, "A novel high-performance mission-enabling multi-purpose radioisotope heat source," in *2022 IEEE Aerospace Conference*, IEEE, 2022.

[17] E. Altenkirch, "Über den nutzeffekt der thermosäule," *Physikalische Zeitschrift*, vol. 10, pp. 560–580, 1909.

[18] E. Altenkirch, "Elektrothermische kälteerzeugung und reversible elektrische heizung," *Physikalische Zeitschrift*, vol. 12, pp. 920–924, 1911.

[19] A. F. Ioffe, L. Stil'Bans, E. Iordanishvili, T. Stavitskaya, A. Gelbtuch, and G. Vineyard, "Semiconductor thermoelements and thermoelectric cooling," *Physics Today*, vol. 12, no. 5, p. 42, 1959.

[20] P. G. Lau and R. J. Buist, "Calculation of thermoelectric power generation performance using finite element analysis," in *XVI ICT'97. Proceedings ICT'97. 16th International Conference on Thermoelectrics (Cat. No. 97TH8291)*, pp. 563–566, IEEE, 1997.

[21] P. Ponnusamy, J. de Boor, and E. Müller, "Using the constant properties model for accurate performance estimation of thermoelectric generator elements," *Applied Energy*, vol. 262, p. 114587, 2020.

[22] G. W. Sutton, *Direct energy conversion*. New York, McGraw-Hill Book Company, 1966.

[23] S. W. Angrist, *Direct energy conversion*. Allyn and Bacon, Inc., Boston, 1976.

[24] E. J. Sandoz-Rosado, S. J. Weinstein, and R. J. Stevens, "On the thomson effect in thermoelectric power devices," *International Journal of Thermal Sciences*, vol. 66, pp. 1–7, 2013.

[25] J. Chen, Z. Yan, and L. Wu, "The influence of thomson effect on the maximum power output and maximum efficiency of a thermoelectric generator," *Journal of applied physics*, vol. 79, no. 11, pp. 8823–8828, 1996.

[26] G. Fraisse, J. Ramousse, D. Sgorlon, and C. Goupil, "Comparison of different modeling approaches for thermoelectric elements," *Energy conversion and management*, vol. 65, pp. 351–356, 2013.

[27] A. Chakraborty, B. Saha, S. Koyama, and K. Ng, "Thermodynamic modelling of a solid state thermoelectric cooling device: Temperature–entropy analysis," *International Journal of Heat and Mass Transfer*, vol. 49, no. 19, pp. 3547–3554, 2006.

[28] C. A. Domenicali, "Irreversible thermodynamics of thermoelectricity," *Reviews of Modern Physics*, vol. 26, no. 2, p. 237, 1954.

[29] C. A. Domenicali, "Stationary temperature distribution in an electrically heated conductor," *Journal of Applied Physics*, vol. 25, no. 10, pp. 1310–1311, 1954.

[30] J. Brittain, "Thevenin's theorem," *IEEE Spectrum*, vol. 27, no. 3, pp. 42–, 1990.

[31] S. E. Wielgosz, C. E. Clifford, K. Yu, and M. M. Barry, "Fully-coupled thermal-electric modeling of thermoelectric generators." Unpublished, 2022.

[32] C. E. Clifford, S. Sammak, and M. Barry, "Model form and discretization uncertainty of thermal-fluid-electric coupled thermoelectric systems," in *ASTFE Digital Library*, Begel House Inc., 2021.

[33] Z. Tang, L. Hu, T. Zhu, X. Liu, and X. Zhao, "High performance n-type bismuth telluride based alloys for mid-temperature power generation," *Journal of Materials Chemistry C*, vol. 3, no. 40, pp. 10597–10603, 2015.

[34] D. Wu, L.-D. Zhao, S. Hao, Q. Jiang, F. Zheng, J. W. Doak, H. Wu, H. Chi, Y. Gelbstein, C. Uher, *et al.*, "Origin of the high performance in gete-based thermoelectric materials upon bi2te3 doping," *Journal of the American Chemical Society*, vol. 136, no. 32, pp. 11412–11419, 2014.